ISSN 2072-5981
doi: 10.26907/mrsej

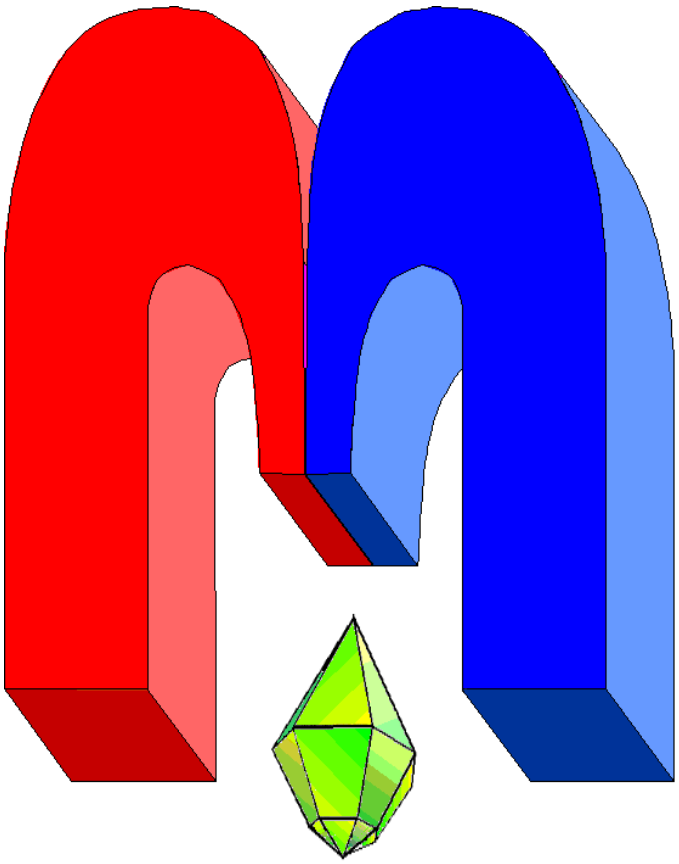

Magnetic Resonance in Solids

Electronic Journal

Volume ***26***
Issue ***1***
Article No ***24102***
1-11 pages
April, ***19***
2024
doi: **10.26907/mrsej-24102**

http://mrsej.kpfu.ru
https://mrsej.elpub.ru

Established and published by Kazan University*
Endorsed by International Society of Magnetic Resonance (ISMAR)
Registered by Russian Federation Committee on Press (#015140), August 2, 1996
First Issue appeared on July 25, 1997

"***Magnetic Resonance in Solids. Electronic Journal***" (**MRS*ej***) is a peer-reviewed, all electronic journal, publishing articles which meet the highest standards of scientific quality in the field of basic research of a magnetic resonance in solids and related phenomena.

Indexed and abstracted by
Web of Science (*ESCI*, Clarivate Analytics, from 2015), *Scopus* (Elsevier, from 2012), *RusIndexSC* (*eLibrary*, from 2006), *Google Scholar*, *DOAJ*, *ROAD*, *CyberLeninka* (from 2006), *SCImago Journal & Country Rank*, etc.

* Address: "Magnetic Resonance in Solids. Electronic Journal", Kazan Federal University; Kremlevskaya str., 18; Kazan 420008, Russia

† In Kazan University the Electron Paramagnetic Resonance (EPR) was discovered by Zavoisky E.K. in 1944.

Short cite this: *Magn. Reson. Solids* **26**, 24102 (2024) doi: 10.26907/mrsej-24102

Paramagnon excitations' theory for nuclear magnetic resonance and resonant inelastic X-ray scattering studies in doped plane copper oxide superconductors†

I.A. Larionov

Kazan Federal University, Kazan 420008, Russia

E-mail: Larionov.MRSLab@mail.ru

(Received March 15, 2024; accepted April 15, 2024; published April 19, 2024)

A mini auto-review of relaxation function theory with paramagnon excitations for doped $S = 1/2$ two-dimensional Heisenberg antiferromagnetic system is given in view of magnetic response of high-T_c copper oxide superconductors as obtained by nuclear magnetic resonance (NMR) and resonant inelastic X-ray scattering (RIXS). It is shown that RIXS data analysis is affected by approximations made for dynamic spin susceptibility and thus depends on paramagnon damping. The results of the theory give fair agreement without especially adjusted parameters to RIXS data for Y-Ba-Cu-O and Nd(La)-Ba(Sr)-Cu-O family compounds.

PACS: 74.72.-h, 75.40.Gb
Keywords: dynamic spin susceptibility, NMR, RIXS

1. Introduction

The main research of magnetic properties of copper oxide high-temperature superconductors (high-T_c) has been focused on evolution of spin excitations from antiferromagnetic (AF) state to superconducting (SC) state with doping [1–4]. In the carrier free systems the elementary excitations in high-T_c's are spin waves (magnons in the quasiparticle language) [5–7]. This concept has been thoroughly investigated in the past [8] and now is widely used for description of two-dimensional (2D) (anti-)ferromagnets. It is therefore tempting to consider the doped 2D Heisenberg AF (2DHAF) systems in terms of paramagnon excitations, a notation used for spin fluctuations in representation of *damped* spin waves in the non-ordered, paramagnetic phase or, if we want to be cautious, paramagnon-like excitations. In the optimally doped (maximum T_c) high-T_c's the motion of charge carriers is known to take place in the presence of strong AF fluctuations [9, 10] and spin waves in 2DHAF systems persist even without long range order in the paramagnetic state [5–8, 11]. The concept of damped spin waves, paramagnons in the quasiparticle language, is therefore appears to be the clue in explaining the spin dynamics in normal, non superconducting, state of plane copper oxide high-T_c's [1, 12, 13] and shall be accounted for in the present studies down to the superconducting state.

In this mini auto-review we will show that description of recent RIXS experiments together with nuclear spin-lattice relaxation data as obtained by nuclear magnetic/quadrupole resonance (NMR/NQR) can be obtained within the relaxation function theory and without parameters especially adjusted to the RIXS data [14, 15].

Experimental research of doped cuprates has been focused mainly on low energy elementary excitations in narrow range of wave vectors of the Brillouin zone because of technique limitations. Recent Resonant Inelastc X-ray Scattering (RIXS) experiments [13, 16] gave information about the imaginary part of dynamic spin susceptibility along the [100] direction and are complementary to neutron scattering (NS) studies that are focused mainly on the wave vectors around the AF wave vector $\mathbf{Q} = (\pi, \pi)$. The general theory of RIXS by collective magnetic excitations is

†This paper is dedicated to Professor Boris I. Kochelaev on the occasion of his 90th birthday.

given by Haverkort [17].

For underdoped $YBa_2Cu_3O_{6.35}$ with $T_c = 18\,K$, where the magnetic excitations are very similar to that of carrier free 2DHAF systems, evidence for spin waves was reliably obtained from NS studies [18]. In the nearly optimally doped $YBa_2Cu_3O_{6.85}$ NS studies showed that AF spin excitations of copper oxide high-T_c emanate in the overall doping range from those of the parent insulator, i.e., the spin waves [19].

In the majority of superconducting cuprates RIXS data confirmed the existence of paramagnon excitations [13, 16] and properties that correspond to the presence of damped spin excitations (paramagnons) with dispersion that is close to magnons in cuprates without charge carriers – AF insulators. For all studied systems the experimental spectra covered a wide range of compounds and doping levels: AF carrier-free $Nd_{1.2}Ba_{1.8}Cu_3O_6$, heavily underdoped $Nd_{1.2}Ba_{1.8}Cu_3O_7$ and $YBa_2Cu_3O_{6.6}$ (with $T_c = 65\,K$ and $61\,K$, respectively), underdoped $YBa_2Cu_4O_8$ ($T_c = 80\,K$) and lightly overdoped $YBa_2Cu_3O_7$ ($T_c = 90\,K$), and $La_{2-x}Sr_xCuO_4$ from underdoped, $x = 0$, to heavily overdoped $x = 0.4$ regimes, that proves the existence of damped paramagnons, that is, clearly well-defined magnetic excitations of cuprates with various doping levels. In [20] we showed that the so called "resonance peak" feature from the underdoped up to the optimally doped regime of high-T_c copper oxides at low temperatures seen by NS is caused to a large degree by the paramagnon-like properties and explanation of ω/T scaling of the averaged over the Brillouin zone imaginary part of dynamic spin susceptibility in lightly doped copper oxide high-T_c compounds does not require the concept of putative quantum critical point. The approximations we used were within the Markovian approximation and "... by itself the Markovian situation can be valid even in the absence of any picture of the system in terms of well-defined excitations" [11].

2. Basic relations

The $t-J$ model Hamiltonian [21, 22] known as the minimal model for the electronic properties of high-T_c cuprates

$$H_{t-J} = \sum_{i,j,\sigma} t_{ij} X_i^{\sigma 0} X_j^{0\sigma} + J \sum_{i>j} (\mathbf{S}_i \mathbf{S}_j - \frac{1}{4} n_i n_j), \tag{1}$$

is written in terms of the Hubbard electron creation (annihilation) operators $X_i^{\sigma 0}$ ($X_i^{0\sigma}$) with spin σ at site i and $\mathbf{S}_i$ are spin-1/2 operators. The hopping integral $t_{ij} = t = J/0.2$ between the nearest neighbors (NN) describes the motion of electrons causing a change in their spins and $J = 0.12\,eV$ is the NN AF coupling constant. The spin and density operators are defined as follows: $S_i^{\sigma} = X_i^{\sigma\tilde{\sigma}}$, $S_i^z = (1/2)\sum_\sigma \sigma X_i^{\sigma\sigma}$, $n_i = \sum_\sigma X_i^{\sigma\sigma}$, $(\sigma = -\tilde{\sigma})$, with the standard normalization $X_i^{00} + X_i^{++} + X_i^{--} = 1$.

We will formulate our study of spin fluctuations following Mori [23], who showed it's efficiency for both the classical (and essential equivalence to Brownian motion) and quantum (e.g., Heisenberg systems of arbitrary dimension) many body systems [11]. This formulation in terms of relaxation functions is related to mean field Green's function technique [11]. The time evolution of a dynamical variable $S_{\mathbf{k}}^z(\tau)$, say, is given by the equation of motion,

$$\dot{S}_{\mathbf{k}}^z(\tau) \equiv \frac{dS_{\mathbf{k}}^z(\tau)}{d\tau} = i\mathcal{L}S_{\mathbf{k}}^z(\tau) \to [H_{t-J}, S_{\mathbf{k}}^z(\tau)], \tag{2}$$

where the Liouville superoperator $\mathcal{L}$ in the quantal case represents the commutator with the Hamiltonian. The projection of the vector $S_{\mathbf{k}}^z(\tau)$ onto the $S_{\mathbf{k}}^z \equiv S_{\mathbf{k}}^z(\tau = 0)$ axis, $\mathcal{P}_0 S_{\mathbf{k}}^z(\tau) = \mathcal{R}(\mathbf{k}, \tau) S_{\mathbf{k}}^z$, defines the linear projection Hermitian operator $\mathcal{P}_0$. The operator $S_{\mathbf{k}}^z(\tau)$ may be

separated into the projective and vertical components $S^z_{\mathbf{k}}(\tau) = \mathcal{R}(\mathbf{k},\tau)S^z_{\mathbf{k}} + (1-\mathcal{P}_0)S^z_{\mathbf{k}}(\tau)$ with respect to the $S^z_{\mathbf{k}}$ axis, where

$$\mathcal{R}(\mathbf{k},\tau) \equiv (S^z_{\mathbf{k}}(\tau),(S^z_{-\mathbf{k}})^*)(S^z_{\mathbf{k}},(S^z_{-\mathbf{k}})^*)^{-1}$$

is the relaxation function in the inner-product bracket notation:

$$(S^z_{\mathbf{k}}(\tau),(S^z_{-\mathbf{k}})^*) \equiv k_{\mathrm{B}}T\int_0^{1/k_{\mathrm{B}}T} d\varrho\,\langle e^{\varrho H}S^z_{\mathbf{k}}(\tau)e^{-\varrho H}(S^z_{-\mathbf{k}})^*\rangle,$$

and the angular brackets denote the thermal average.

The Laplace transform of the relaxation function may be presented in a form of continued fraction, for which Lovesey and Meserve [11, 24] used a three pole approximation,

$$\mathcal{R}^L(\mathbf{k},s) = \int_0^\infty d\tau\, e^{-s\tau}\mathcal{R}(\mathbf{k},\tau) \approx 1/\{s+\Delta^2_{1\mathbf{k}}/[s+\Delta^2_{2\mathbf{k}}/(s+1/\tau_{\mathbf{k}})]\},$$

with a cutoff characteristic time $\tau_{\mathbf{k}} = \sqrt{2/(\pi\Delta^2_{2\mathbf{k}})}$, by arguing that $S^z_{\mathbf{k}}(\tau)$ fluctuations are weakly affected by the higher order random forces. For the relaxation shape function $\mathcal{F}(\mathbf{k},\omega) = \mathrm{Re}[\mathcal{R}^L(\mathbf{k},i\omega)]/\pi$, this gives

$$\mathcal{F}(\mathbf{k},\omega) = \frac{1}{\pi}\frac{\tau_{\mathbf{k}}\Delta^2_{1\mathbf{k}}\Delta^2_{2\mathbf{k}}}{[\omega\tau_{\mathbf{k}}(\omega^2-\Delta^2_{1\mathbf{k}}-\Delta^2_{2\mathbf{k}})]^2+(\omega^2-\Delta^2_{1\mathbf{k}})^2}, \tag{3}$$

where $\Delta^2_{1\mathbf{k}}$ and $\Delta^2_{2\mathbf{k}}$ are related to the frequency moments,

$$\langle\omega^n_{\mathbf{k}}\rangle = \int_{-\infty}^{\infty} d\omega\,\omega^n\mathcal{F}(\mathbf{k},\omega) = (1/i^n)\left[d^n\mathcal{R}(\mathbf{k},\tau)/d\tau^n\right]_{\tau=0},$$

of $\mathcal{R}(\mathbf{k},\tau)$ as $\Delta^2_{1\mathbf{k}} = \langle\omega^2_{\mathbf{k}}\rangle$, $\Delta^2_{2\mathbf{k}} = \langle\omega^4_{\mathbf{k}}\rangle / \langle\omega^2_{\mathbf{k}}\rangle - \langle\omega^2_{\mathbf{k}}\rangle$ for $\tau > \tau_{\mathbf{k}}$. Note that $\mathcal{F}(\mathbf{k},\omega)$ is real, normalized to unity $\int_{-\infty}^{\infty} d\omega\mathcal{F}(\mathbf{k},\omega) = 1$ and is even in both $\mathbf{k}$ and ω. The expression for the second moment,

$$\langle\omega^2_{\mathbf{k}}\rangle = i\langle[\dot{S}^z_{\mathbf{k}},S^z_{-\mathbf{k}}]\rangle/\chi(\mathbf{k}) = -(8Jc_1 - 4t_{\mathrm{eff}}T_1)(1-\gamma_{\mathbf{k}})/\chi(\mathbf{k}),$$

is compact, while $\langle\omega^4_{\mathbf{k}}\rangle = i\langle[\ddot{S}^z_{\mathbf{k}},\dot{S}^z_{-\mathbf{k}}]\rangle/\chi(\mathbf{k})$ is cumbersome and is not reproduced here (see Ref. [25] for details).

Within the $t-J$ model the static spin susceptibility $\chi(\mathbf{k})$ in the overall temperature and doping range is given by [26]

$$\chi(\mathbf{k}) = \frac{4|c_1|}{Jg_-(g_+ + \gamma_{\mathbf{k}})}, \tag{4}$$

and has the same structure as in the isotropic spin-wave theory [27]. The correlation length ξ is related to the parameter g_+ via the expression $\xi/a = 1/(2\sqrt{g_+-1})$, where $a = 3.8$ Å is a lattice unit. The spin-spin correlation function between NN is defined as

$$c_1 = \frac{1}{4}\sum_{\boldsymbol{\rho}}\langle S^z_j S^z_{j+\boldsymbol{\rho}}\rangle,$$

the transfer amplitude between the NN is given by:

$$T_1 \equiv -\frac{1}{4}\sum_{\boldsymbol{\rho}}\left\langle X^{\sigma 0}_i X^{0\sigma}_{i+\boldsymbol{\rho}}\right\rangle = p\sum_{\mathbf{k}}\gamma_{\mathbf{k}}f^h_{\mathbf{k}},$$

where

$$\gamma_{\mathbf{k}} = \frac{1}{4}\sum_{\boldsymbol{\rho}} \exp(i\mathbf{k}\boldsymbol{\rho}) = \frac{1}{2}(\cos k_x a + \cos k_y a),$$

the index $\boldsymbol{\rho}$ runs over NN, and $f^h_{\mathbf{k}} = [\exp(-E_{\mathbf{k}}+\mu)/k_{\mathrm{B}}T+1]^{-1}$ is the Fermi function of holes. The number of *extra* holes, due to doping, δ, per one plane Cu^{2+}, can be identified with the Sr content x in $La_{2-x}Sr_xCuO_4$. The chemical potential μ is related to δ by $\delta = p\sum_{\mathbf{k}} f^h_{\mathbf{k}}$, where $p = (1+\delta)/2$. The excitation spectrum of holes is given by $E_{\mathbf{k}} = 4\,t_{\mathrm{eff}}\,\gamma_{\mathbf{k}}$, where the hoppings, t, are affected by electronic and AF spin-spin correlations c_1, resulting in *effective* values [21,22,28,29], for which we set $t_{\mathrm{eff}} = \delta J/0.2$ in order to match the insulator-metal transition. This renormalization of hopping may be easily understood because a hole when moving through the lattice retains its spin orientation. The temperature and doping dependence of the parameters of the theory, g_- and c_1, have been calculated selfconsistently.

For low temperature behavior we use the expression, resulting in *effective* correlation length ξ_{eff}, given by [25,28,30]

$$\xi^{-1}_{\mathrm{eff}} = \xi^{-1}_0 + \xi^{-1}. \tag{5}$$

Here, ξ is affected by doped holes, in contrast with the Keimer *et al.* [30] empirical equation, where ξ is given by the Hasenfratz-Niedermayer formula and there was no influence of the hole subsystem on ξ. Thus from now on we replace ξ by ξ_{eff}. For doped systems we use the explicit expression [26] for ξ which is much more complicated compared with simple relation

$$\xi/a \simeq (J\sqrt{g_-}/k_{\mathrm{B}}T)\exp(2\pi\rho_S/k_{\mathrm{B}}T),$$

valid for carrier free or lightly doped systems [26]. In the best fit of ξ_{eff} to experimental data [30, 31] the relation $\xi_0 = a/n_\xi x$ is most suited [20,25] which one may attribute to stripe picture, where $n_\xi = 2$ for $x \leq 0.05$ and $n_\xi = 1$ near optimal ($x \approx 0.15$) doping. The results of the calculations are summarized in Table 1.

Table 1. The calculated at $T = 300\,\mathrm{K}$ AF spin-spin correlation function c_1, the parameter g_-, the spin stiffness constant ρ_S. All these quantities have weak temperature dependence. The last column shows the value of AF correlation length used in the limit $T \to 0$

x	c_1	g_-	$2\pi\rho_S/J$	ξ_0
0	-0.1152	4.1448	0.38	-
0.04	-0.1055	3.913	0.3	$1/(2\delta)$
0.115	-0.0758	3.252	0.2	$1/\delta$
0.15	-0.0617	2.947	0.13	$1/\delta$

The temperature and doping dependence of the paramagnon excitations may be studied further since the relaxation function can be understood within the spin-wave framework [11].

The relaxation shape function (3) in the *undamped* regime is directly related to the imaginary part of dynamic spin susceptibility $\chi''(\mathbf{k},\omega)$ as [11],

$$\chi''(\mathbf{k},\omega) = \omega\chi(\mathbf{k})F(\mathbf{k},\omega). \tag{6}$$

Alternatively, in the *damped* regime, the dispersion of paramagnon excitations, renormalized by interactions, is given by the relaxation shape function [11],

$$\omega^{\mathrm{sw}}_{\mathbf{k}} = 2\int_0^\infty d\omega\,\omega\mathcal{F}(\mathbf{k},\omega), \tag{7}$$

where the integration over ω in (7) has been performed analytically and exactly and the damping of paramagnon excitations is given by

$$\Gamma_{\mathbf{k}} = \sqrt{\langle \omega_{\mathbf{k}}^2 \rangle - (\omega_{\mathbf{k}}^{\rm sw})^2}. \tag{8}$$

3. Results and discussion

Having established the paramagnon dispersion and damping we now proceed with calculations of imaginary part of the dynamic spin susceptibility.

The nuclear spin-lattice relaxation rate $1/T_1$ is given by

$$^{\alpha}(1/T_1) = \frac{2k_{\rm B}T}{\omega_0} \sum_{\mathbf{k}}^{\alpha} F(\mathbf{k})^2 \chi''(\mathbf{k}, \omega_0), \tag{9}$$

where $\omega_0 \ll T, J$ is the measuring NMR/NQR frequency. The quantization axis of the electric field gradient coincides with the crystal axis c which is perpendicular to CuO_2 planes defined by a and b. The wave vector dependent hyperfine formfactor for plane ^{63}Cu sites [32, 33] is given by, $^{63}F(\mathbf{k})^2 = (A_{ab} + 4\gamma_{\mathbf{k}}B)^2$, where $A_{ab} = 1.7 \cdot 10^{-7}$ eV and $B = (1 + 4x) \cdot 3.8 \cdot 10^{-7}$ eV are the Cu on-site and transferred hyperfine couplings, respectively. The relation for B is used to match the weak changes with Sr doping [36].

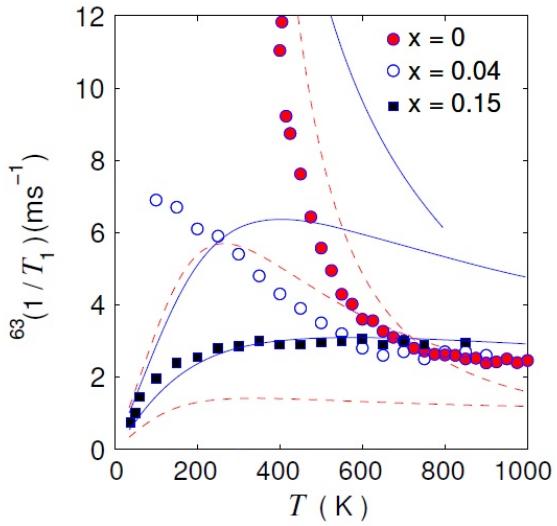

Figure 1. The calculated temperature dependencies of plane copper nuclear spin-lattice relaxation rate $^{63}(1/T_1) = 2W$ in $La_{2-x}Sr_xCuO_4$ (data from [34]) for $x = 0.0$, $x = 0.04$ and $x = 0.15$ in the approximation for undamped paramagnon-like excitaions, Eq.(6) (dashed lines), and by solid lines for $\chi''_{L1}(\mathbf{q}, \omega)$ with damping (Lorentzian form 1, Eq.(10)) [15].

Figure 1 shows the temperature dependencies of plane copper nuclear spin-lattice relaxation rate, $^{63}(1/T_1)$. Equations (4)-(6), (9), and Figure 1 show that the temperature dependence of $^{63}(1/T_1)$ is mainly governed by the temperature dependence of the AF correlation length and by the factor $k_{\rm B}T$. At low T, where $\xi_{\rm eff} \simeq$ const, the plane copper $^{63}(1/T_1) \propto T$, as it should. At high T, the correlation length shows weak doping dependence and behaves similarly to that of carrier free La_2CuO_4 and therefore $^{63}(1/T_1)$ of doped samples behaves similarly to that of La_2CuO_4. Thus our results suggest that the "pseudogap" effect seen by NMR in the high-T_c cuprates is *hidden* in the correlation length that affects the observable quantities, and, generally, is in agreement with the conclusion based on the nearly AF Fermi liquid concept [35, 36] about the leading role of the correlation length in temperature and doping dependence of $1/T_1$.

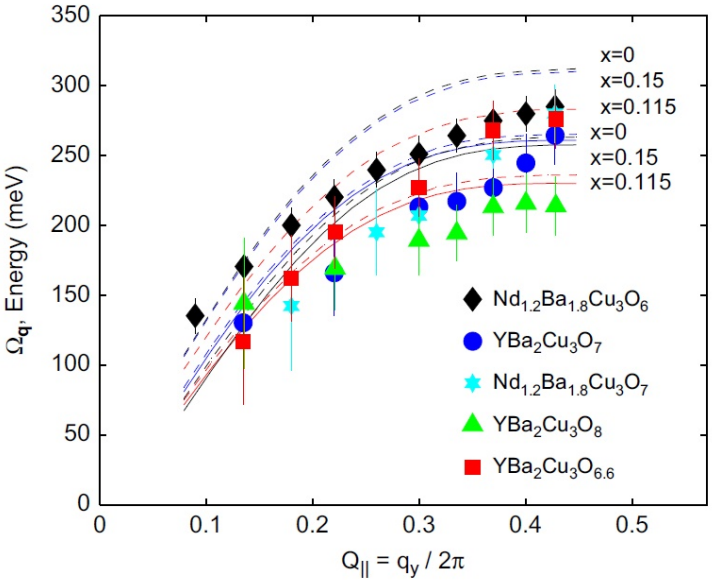

Figure 2. Experimental data for dispersion of paramagnon excitations along the (0,0)-(π,0) axis as obtained by RIXS are from [13]. Dashed and dash-dotted lines show calculations of dispersion of paramagnon-like excitations with damping following Eq. 10 and Eq. 12, respectively. Solid lines show calculations of paramagnon dispersion given by Eq. 7. All calculated values for $x = 0$ and $x = 0.15$ are nearly the same [14].

Resonant inelastic X-ray scattering measures the maximum of imaginary part of the dynamic spin susceptibility at a certain wave vector. As we will show below, the results of RIXS data analysis depend significantly on the specific analytical expression for imaginary part of the dynamic spin susceptibility. Here we will consider three (a,b,c) somewhat similar approaches. This result implies that we have to be cautious when interpreting the RIXS data (see Figure 2) as a direct measurement of (para-)magnon dispersion. We note that the calculations are carried out without any fitting parameters to the RIXS data.

a) *Lorentzian form 1* of the imaginary part of the dynamic spin susceptibility [37],

$$\chi''_{L1}(\mathbf{k},\omega) = \frac{\chi(\mathbf{k})\omega\Gamma_{\mathbf{k}}}{(\omega-\omega^{\rm sw}_{\mathbf{k}})^2+\Gamma^2_{\mathbf{k}}} + \frac{\chi(\mathbf{k})\omega\Gamma_{\mathbf{k}}}{(\omega+\omega^{\rm sw}_{\mathbf{k}})^2+\Gamma^2_{\mathbf{k}}}, \tag{10}$$

is asymmetric in frequency ω, at it should. From the frequency dependence it follows that (10) has maximum with the following condition,

$$\Omega_{\mathbf{k}} = \omega_{\rm Res} = \sqrt{(\omega^{\rm sw}_{\mathbf{k}})^2+\Gamma^2_{\mathbf{k}}}, \tag{11}$$

implying that $\chi''_{L1}(\mathbf{k},\omega)$ maximum value as seen by RIXS is strongly affected by the damping $\Gamma_{\mathbf{k}}$.

b) *Lorentzian form 2* of the imaginary part of the dynamic spin susceptibility has a somewhat similar structure [13],

$$\chi''_{AL}(\mathbf{k},\omega) \propto \frac{\Gamma_{\mathbf{k}}}{(\omega-\omega^{\rm sw}_{\mathbf{k}})^2+\Gamma^2_{\mathbf{k}}} - \frac{\Gamma_{\mathbf{k}}}{(\omega+\omega^{\rm sw}_{\mathbf{k}})^2+\Gamma^2_{\mathbf{k}}}, \tag{12}$$

which is asymmetric in frequency also, and its frequency ω dependence dictates that (12) has maximum at

$$\Omega_{\mathbf{k}} = \omega_{AL,\rm Res} = \frac{1}{\sqrt{3}}\sqrt{(\omega^{\rm sw}_{\mathbf{k}})^2-\Gamma^2_{\mathbf{k}}+2\sqrt{(\omega^{\rm sw}_{\mathbf{k}})^4+\Gamma^4_{\mathbf{k}}+(\omega^{\rm sw}_{\mathbf{k}})^2\Gamma^2_{\mathbf{k}}}} > \omega^{\rm sw}_{\mathbf{k}}, \tag{13}$$

that is rather different from the result with *Lorentzian form 1* (10). In the limit of small damping $\Gamma_{\mathbf{k}} < \omega^{\rm sw}_{\mathbf{k}}$ this gives

$$\omega_{AL,\rm Res} \approx \omega^{\rm sw}_{\mathbf{k}} \left[1 + \frac{\Gamma^4_{\mathbf{k}}}{6(\omega^{\rm sw}_{\mathbf{k}})^4}\right]. \tag{14}$$

Figure 2 shows that result with *Lorentzian form 2* (12) in our case is indeed very close to bare paramagnon excitations dispersion.

c) *A simpler approach* for dynamic spin susceptibility, i.e.,

$$\chi(\mathbf{k},\omega) = \eta_{\mathbf{k}}/[(\omega^{\rm sw}_{\mathbf{k}})^2 - \omega^2 + i\Gamma_{\mathbf{k}}\omega] \tag{15}$$

gives the maximum at

$$\omega_{S,\rm Res} \approx \omega^{\rm sw}_{\mathbf{k}} \left[1 - \frac{\Gamma^2_{\mathbf{k}}}{8(\omega^{\rm sw}_{\mathbf{k}})^2}\right] \tag{16}$$

for $\Gamma_{\mathbf{k}} < \omega^{\rm sw}_{\mathbf{k}}$. This equation for susceptibility maximum condition gives the correction to $\omega^{\rm sw}_{\mathbf{k}}$ that has the opposite sign compared with the former cases.

This suggests that the RIXS data analysis is strongly affected by damping of paramagnon excitations. We therefore caution against interpreting the RIXS results as exact measurement of (para-)magnon dispersion. The result would eventually include the damping and its effect depends on approximations made when deriving the specific expression for dynamic spin susceptibility.

Figure 2 shows the dispersion of paramagnon excitations along the line (0,0) - (π,0). Experimental data for dispersion of paramagnon excitations in antiferromagnetic $Nd_{1.2}Ba_{1.8}Cu_3O_6$, underdoped $Nd_{1.2}Ba_{1.8}Cu_3O_7$, $YBa_2Cu_3O_{6.6}$, $YBa_2Cu_4O_8$ and $YBa_2Cu_3O_7$ at $T = 15\,$K are taken from [13]. The results of the calculations (lines) are given for several doping values, designated by the value of charge carriers concentration, x. Dashed lines - calculation with use of *Lorentzian form 1* for imaginary part of a dynamic spin susceptibility that takes into account thermal damping of paramagnon excitations (10). Dash-dotted lines show the same for *Lorentzian form 2* (12). The latter result is very close to that for bare paramagnon dispersion, given by 7 and shown by solid lines.

The wavevector dependence of paramagnon dispersion $\omega^{\rm sw}_{\mathbf{k}}$ (Figures 3a, 4a) and damping $\Gamma_{\mathbf{k}}$ (Figures 3b, 4b), respectively, is shown for the cases of pure AF and optimal doping, and at various temperatures. Both quantities have weak temperature dependence below $T < J/2$ except for region around values of AF wave vector $Q_{\rm AF} = (\pi,\pi)$. Both Figures 3a and 4a show gradual paramagnon softening with doping and temperature.

In our theory we do not assume any putative Quantum Critical Point (QCP) scenario – phase transition at $T = 0$ and nearly optimal doping $x \approx 0.15$. Earlier this QCP was invented as the source of "exotic" properties of high-T_c compounds, including the "dome"-like dependence of T_c in the temperature-doping index phase diagram, and the ω/T scaling, nearly universal behavior of averaged over the Brillouin zone the imaginary part of dynamic spin susceptibility, in light doping regime. Our findings are in agreement with conclusion of Ref. [16] about the absence of sharp changes in the high-energy magnetic fluctuations that might be expected in the presence of hidden quantum critical point.

Figure 5 shows the temperature dependence of damping $\Gamma_{\mathbf{Q}}$ for paramagnon excitations at AF wave vector $Q_{\rm AF} = (\pi,\pi)$ at various doping levels, x. The nearly square-law for $\Gamma_{\mathbf{Q}}$ versus

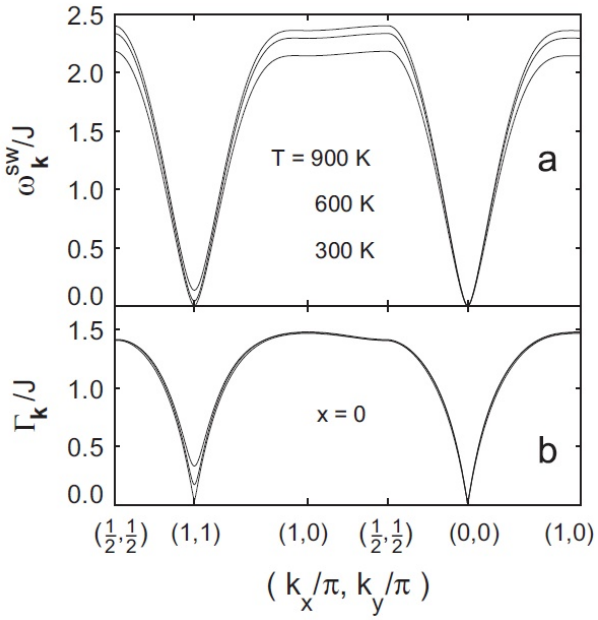

Figure 3. a) Dispersion $\omega^{\rm sw}_{\mathbf{k}}$ and b) damping $\Gamma_{\mathbf{k}}$ of paramagnon excitations along a contour $(\pi/2,\pi/2)$ – (π,π) – $(\pi,0)$ – $(\pi/2,\pi/2)$ – (0,0) – $(\pi,0)$ for a pure Heisenberg antiferromagnet, $x = 0$ [14].

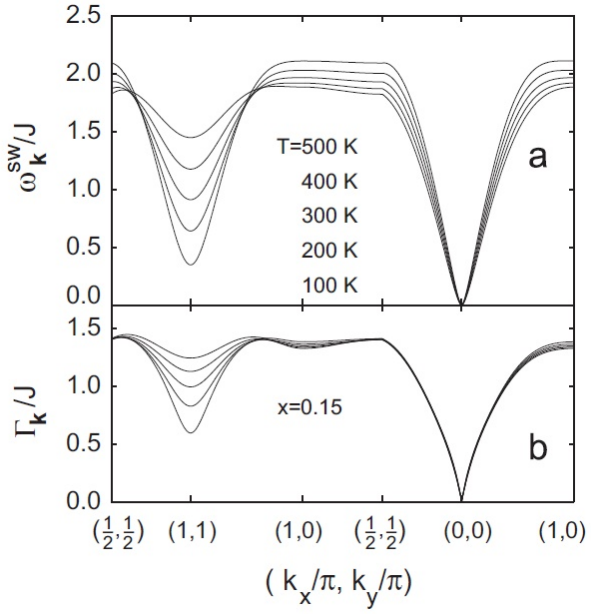

Figure 4. a) Dispersion $\omega^{\rm sw}_{\mathbf{k}}$ and b) damping $\Gamma_{\mathbf{k}}$ of paramagnon excitations along a contour $(\pi/2,\pi/2)$ – (π,π) – $(\pi,0)$ – $(\pi/2,\pi/2)$ – (0,0) – $(\pi,0)$ for doping near optimal, $x = 0.15$ [14].

temperature for pure AF is in qualitative agreement with results of Refs. [38,39]. At low doping, $x \approx 0.04$, the results of the calculations are in agreement with conclusion made in Ref. [40], that the linear dependence of damping versus temperature is necessary to explain the ω/T scaling of averaged over the Brillouin zone the imaginary part of dynamic spin susceptibility, experimentally observed by NS in low doped, $0.02 < x < 0.05$ samples. For doping near optimal, $x \approx 0.15$, Figure 5 shows that the damping continues to exhibit the dramatic change of temperature dependence, $\Gamma_{\mathbf{Q}} \propto \sqrt{T}$.

The half width at half maximum (HWHM) of magnetic excitations is within 200–250 meV [13]

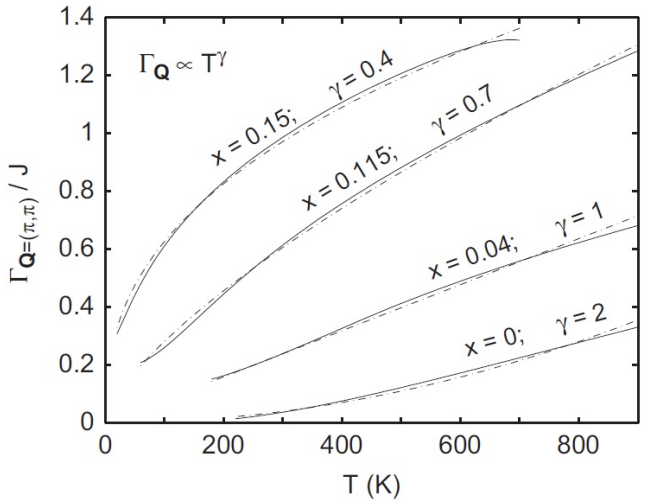

Figure 5. Temperature dependence of damping parameter $\Gamma_{\mathbf{Q}}$ for paramagnon(-like) excitations at AF wave vector $\mathbf{Q} = (\pi, \pi)$ at various doping levels, x. Solid lines show the results of the calculations, dashed lines show the result of the fit with $\Gamma_{\mathbf{Q}} \propto T^{\gamma}$ with power index γ as shown near the curves [14].

for numerous cuprates and within 50–200 meV [16] for undoped, underdoped and optimally doped $La_{2-x}Sr_xCuO_4$ compounds in the region of the wave vectors $0.2 \leq Q_{||} \leq 0.4$. The calculated values of damping versus $\mathbf{k}$ in this region $\Gamma \approx 1.4J \approx 170$ meV are in quantitative agreement with these experimental data.

Our findings are in general agreement also with [17, 41, 42] that support the magnetic excitations scenario for RIXS studies of doped high-T_c copper oxides. The exact diagonalization and Monte Carlo studies of Jia *et al.* [42] showed that the magnetic excitations have the same dispersion as shown experimentally and in the present work. However, their calculations were performed at $T \approx 1500$ K that is inaccessible experimentally and is beyond our current interest.

4. Conclusion

In conclusion we showed that the magnetic properties of high-T_c copper oxides in the normal, nonsuperconducting state as obtained by RIXS, nuclear magnetic resonance and neutron scattering, can be explained in unified form by relaxation function theory. RIXS data analysis is strongly affected by damping of paramagnon excitations and we therefore caution against interpreting the RIXS results as exact measurement of (para-)magnon dispersion since it will depend on the specific expression for dynamic spin susceptibility. The concept of paramagnon excitations appears to be a natural clue in understanding the normal state of doped high-T_c copper oxides.

5. Acknowledgments

It is a pleasure to thank Professor B.I. Kochelaev for illuminating lectures on Quantum Theory of Solid State and conference talks.

References

1. Kastner M. A., Birgeneau R. J., Shirane G., Endoh Y. *Rev. Mod. Phys.* **70**, 897 (1998)

2. Eschrig M. *Advances in Physics* **55**, 47 (2006)

3. Chubukov A.V., Pines D., Schmalian J. in *Physics of Superconductors* **1**, 495 (2003)

4. Kivelson S.A., Bindloss I.P., Fradkin E., Oganesyan V., Tranquada J.M., Kapitulnik A., Howald C. *Rev. Mod. Phys.* **75**, 1201 (2003)

5. Chakravarty S., Halperin B. I., Nelson D. R.*Phys. Rev. Lett.* **60**, 1057 (1988)

6. Chakravarty S., Halperin B. I., Nelson D. R.*Phys. Rev. B* **39**, 2344 (1989)

7. Takahashi M.*Phys. Rev. B* **40**, 2494 (1989)

8. Hone D. W., Richards P. M.*Annu. Rev. Mater. Sci.* **4**, 337 (1974)

9. Moriya T., Ueda K. *Adv. Phys.* **49**, 555 (2000)

10. Moriya T., Ueda K. *Rep. Prog. Phys.* **66**, 1299 (2003)

11. Balucani U., Lee M. H., Tognetti V. *Phys. Rep.* **373**, 409 (2003)

12. Larionov I. A. *Phys. Rev. B* **76**, 224503 (2007)

13. Le Tacon M., Ghiringhelli G., Chaloupka J., Moretti Sala M., Hinkov V., Haverkort M. W., Minola M., Bakr M., Zhou K. J., Blanco-Canosa S., Monney C., Song Y. T., Sun G. L., Lin C. T., De Luca G. M., Salluzzo M., Khaliullin G., Schmitt T., Braicovich L., Keimer B. *Nature Physics* **7**, 725 (2011)

14. Larionov I. A. *Solid State Comm.* **208**, 29 (2015)

15. Larionov I. A. *J. of Phys.: Conf. Ser.* **324**, 011001 (2011)

16. Dean M. P. M., Dellea G., Springell R. S., Yakhou-Harris F., Kummer K., Brookes N. B., Liu X., Sun Y-J., Strle J., Schmitt T., Braicovich L., Ghiringhelli G., Bozovic I., Hill J. P. *Nature Materials* **12**, 1019 (2013)

17. Haverkort M. W. *Phys. Rev. Lett.* **105**, 167404 (2010)

18. Stock C., Buyers W. J. L., Yamani Z., Tun Z., Birgeneau R. J., Liang R., Bonn D., Hardy W. N. *Phys. Rev. B* **77**, 104513 (2008)

19. Pailhes S., Sidis Y., Bourges P., Hinkov V., Ivanov A., Ulrich C., Regnault L. P., Keimer B. *Phys. Rev. Lett.* **93**, 167001 (2004)

20. Larionov I. A. *Phys. Rev. B* **72**, 094505 (2005)

21. Anderson P. W. *Science* **235**, 1196 (1987)

22. Baskaran G., Zou Z., Anderson P. W. *Solid State Commun.* **63**, 973 (1987)

23. Mori H. *Prog. Theor. Phys.* **34**, 399 (1965)

24. Lovesey S. W., Meserve R. A. *J. Phys.* **C 6**, 79 (1973)

25. Larionov I. A. *Phys. Rev. B* **69**, 214525 (2004)

26. Zavidonov A. Yu. Brinkmann D. *Phys. Rev. B* **58**, 12486 (1998)

27. Sokol A., Singh R. R. P., Elstner N. *Phys. Rev. Lett.* **76**, 4416 (1996)

28. Zavidonov A. Yu., Larionov I. A., Brinkmann D. *Phys. Rev. B* **61**, 15462 (2000)

29. Plakida N. M., Hayn R., Richard J.-L. *Phys. Rev. B* **51**, 16599 (1995)

30. Keimer B., Belk N., Birgeneau R. J., Cassanho A., Chen C. Y., Greven M., Kastner M. A., Aharony A., Endoh Y., Erwin R. W., Shirane G. *Phys. Rev. B* **46**, 14034 (1992)

31. Aeppli G., Mason T. E., Hayden S. M., Mook H. A., Kulda J. *Science* **278**, 1432 (1997)

32. Mila F., Rice T. M. *Physica C*, **157**, 561 (1989)

33. Shastry B. S. *Phys. Rev. Lett.* **63**, 1288 (1989)

34. Imai T., Slichter C. P., Yoshimura K., Kosuge K. *Phys. Rev. Lett.* **70**, 1002 (1993)

35. Millis A. J., Monien H., Pines D. *Phys. Rev. B*, **42**, 167 (1990)

36. Zha Y., Barzykin V., Pines D. *Phys. Rev. B*, **54**, 7561 (1996)

37. Chou H., Tranquada J. M., Shirane G., Mason T. E., Buyers W. J. L., Shamoto S., Sato M. *Phys. Rev. B* **43**, 5554 (1991)

38. Kopietz P. *Phys. Rev. B* **41**, 9228 (1990)

39. Tyc S., Halperin B. I. *Phys. Rev. B* **42**, 2096 (1990)

40. Mikheyenkov A.V., Barabanov A.F., Kozlov N.A. *Phys. Lett. A* **354**, 320 (2006)

41. Dean M. P. M., James A. J. A., Springell R.S., Liu X., Monney C., Zhou K. J., Konik R. M., Wen J.S., Xu Z. J., Gu G. D., Strocov V. N., Schmitt T., Hill J. P. *Phys. Rev. Lett.* **110**, 147001 (2013)

42. Jia C. J., Nowadnick E. A., Wohlfeld K., Kung Y. F., Chen C.-C., Johnston S., Tohyama T., Moritz B., Devereaux T. P. *Nature Communications* **5**, 3314, (2014)

43. Benjamin D., Klich I., Demler E. *Phys. Rev. Lett.* **112**, 247002 (2014)